Computationally efficient bioelectric field modeling and effects of frequency-dependent tissue capacitance

2011 J. Neural Eng. 8 036017

(http://iopscience.iop.org/1741-2552/8/3/036017)

J. Neural Eng. **8** (2011) 036017 (7pp) doi:10.1088/1741-2560/8/3/036017

Computationally efficient bioelectric field modeling and effects of frequency-dependent tissue capacitance

Brian Tracey[1,3] **and Michael Williams**[2]

[1] Department of Electrical and Computer Engineering, Tufts University, Medford, MA 02155, USA
[2] NeuroMetrix, Inc., Waltham, MA 02451, USA

E-mail: btracey@eecs.tufts.edu

Received 19 February 2011
Accepted for publication 6 April 2011
Published 4 May 2011
Online at stacks.iop.org/JNE/8/036017

Abstract
Standard bioelectric field models assume that the tissue is purely resistive and frequency independent, and that capacitance, induction, and propagation effects can be neglected. However, real tissue properties are frequency dependent, and tissue capacitance can be important for problems involving short stimulation pulses. A straightforward interpolation scheme is introduced here that can account for frequency-dependent effects, while reducing runtime over a direct computation by several orders of magnitude. The exact Helmholtz solution is compared to several approximate field solutions and is used to study neural stimulation. Results show that frequency-independent tissue capacitance always acts to attenuate the stimulation pulse, thereby increasing firing thresholds, while the dispersion effects introduced by frequency-dependent capacitance may decrease firing thresholds.

(Some figures in this article are in colour only in the electronic version)

1. Introduction

Most bioelectric modeling studies make the assumption that the electrical field can be regarded as quasi-static and that capacitive effects can be neglected [1, 2]. These assumptions must be carefully examined for problems involving electrical stimulation of peripheral nerves or brain tissue, as the stimulation waveforms have rapid rise times. An excellent comparison of exact and approximate methods for modeling neural stimulation is given in [3] and concludes that the most questionable assumption made in standard modeling is that capacitive effects are negligible. Capacitance can be expected to be particularly important for problems involving surface electrodes, as skin capacitance is much larger than body tissue capacitance.

Some recent work has included a frequency-independent capacitance term in bioelectric simulations [4, 5]. However, measurements show that capacitance in biological tissues is generally frequency dependent [3, 6], which gives rise to dispersive effects [7]. The quasi-static field equations can be modified to account for frequency-dependent capacitance by including a complex, frequency-dependent conductivity [2]. The equations can then be solved in the frequency domain, with time-domain response found via an inverse transform. This requires solving the field equations at every frequency of the discrete Fourier transform (DFT), which greatly increases the computational load. This 'brute force' approach is manageable for scenarios where analytic solutions are available. For example, a brute force approach was used in [3] to find solutions to a current point source in an infinite homogeneous medium. A brute force solution requiring calculations at 1024 frequencies was also used for a 2D axisymmetric finite element method (FEM) model of brain tissue [5]. However, computational load can become an issue when 3D FEM or other numerical models are required.

Several authors have investigated time-domain finite element methods for including frequency dependence and capacitive effects. A combined time domain/frequency domain solution [7] was developed that requires that the tissue is homogeneous and isotropic. More recently, this work has

[3] Author to whom any correspondence should be addressed.

been extended to yield an exact, direct time-domain solution that can account for frequency-dependent permittivity and can model inhomogeneous tissues [8].

In this paper we offer an alternative, frequency-domain approach. Based on tabulated values of tissue properties [6] we have noted that both the magnitude and phase of the solution varies fairly smoothly with frequency. This suggests the use of an interpolation approach in which the equations are first solved at a smaller number of frequencies, and then interpolated to the DFT frequency bins. A key assumption is that the phase of the solution can be unambiguously interpolated across frequency. An interpolation approach that enforces this assumption is outlined below. Interpolation leads to a reduction in computational time of roughly two orders of magnitude as compared to a full calculation at every DFT frequency.

While this approach is straightforward (and is easily implemented using the output of commercial FEM codes), it does not appear to have previously applied to bioelectric modeling. A frequency-domain approach is computationally attractive when studying the effects of stimulus waveform shape. The FEM model can be run once, after which solutions are calculated via forward and inverse Fourier transforms of the different waveforms weighted by the pre-computed FEM results.

The interpolation approach was used to compare an exact Helmholtz equation solution to various approximate solutions for finite element models. Differences between the exact and approximate solutions are presented below. An additional finding is that the exact Helmholtz solution is as computationally fast as approximate solutions.

Finally, we apply the interpolation method to study the effects of tissue properties on neural firing thresholds. A recent study [5] modeled brain tissue with a frequency-independent capacitive component and showed that capacitance led to increased firing thresholds and up to 20% reduction in activated brain volume. We show below that frequency-independent capacitance (as studied in [5]) will always attenuate the bioelectric field, leading to higher thresholds, while frequency-dependent capacitance causes distortion of the pulse and can lead to lower thresholds. While some measurements show brain tissue as having frequency-dependent capacitance [6], other measurements do not [10]. The work below shows that these differences may lead to different conclusions about the role of tissue capacitance in neural stimulation.

2. Methods

2.1. Bioelectric field equations

The inhomogeneous scalar Helmholtz equation is derived in [3]. The derivation first expresses the electric field $\boldsymbol{E}$ in terms of the vector potential $\boldsymbol{A}$ and scalar potential φ. These quantities are then related to each other through the Lorenz condition. Gauss's law and charge conservation are used to simplify the expression. Written in terms of the complex conductivity, $\sigma_c(\omega) = \sigma(\omega) + j\omega\varepsilon_r(\omega)\,\varepsilon_0$, the field equation is [3]

$$\sigma_c(\omega)\nabla^2\varphi - j\mu\omega\sigma_c^2(\omega)\varphi = \nabla\cdot\boldsymbol{J}, \tag{1a}$$

where σ and ε_r are the conductivity and relative permittivity of the tissue, φ is the potential, $\varepsilon_0 = 8.854 \times 10^{-12}$ F m^{-1} is the permittivity of the vacuum, $\mu = 4\pi \times 10^{-7}$ H m^{-1} is the magnetic permeability, and $\nabla\cdot\boldsymbol{J}$ represents a current source (assumed here to be a point source). As noted, the conductivity and permittivity are assumed to be functions of frequency. Although not shown explicitly above, they can also change spatially (i.e. different parts of the model have different tissue properties).

Boundary conditions for the problem are zero potential ($\varphi = 0$) on the ground electrode; no current flows through tissue/air surfaces; and continuity of current across internal interfaces. Together, (1*a*) and the boundary conditions describe a problem that can be solved numerically to give the electrical potential in the tissue.

Nearly all published studies rely on simplifications of (1*a*). The first simplification that can be made is that propagation effects can be ignored when calculating the electric potential. This is felt to be a good assumption at the distances and frequencies of interest for neural stimulation problems. The simplified equation is then

$$\sigma_c\,(\omega)\,\nabla^2\varphi = \nabla\cdot\boldsymbol{J}. \tag{1b}$$

This solution is denoted QS-RC below as it is quasistatic but both resistive and capacitive effects are retained (i.e. the complex conductivity is used). Solutions based on (1*b*) have been used in [6].

A very common further assumption made in the literature is that capacitive effects are negligible at the frequencies of interest [2]. Under this assumption, the (real) conductivity is used in place of the complex conductivity, giving

$$\sigma\,(\omega)\,\nabla^2\varphi = \nabla\cdot\boldsymbol{J}. \tag{1c}$$

This solution is denoted QS-R below as only resistive terms are retained. Generally, a further assumption is made that a frequency-independent value of conductivity can be used, giving

$$\sigma\nabla^2\varphi = \nabla\cdot\boldsymbol{J}. \tag{1d}$$

This solution is denoted QS-RFI (resistive frequency-independent). It is by far the most widely used approximation to equation (1*a*) (see [9] for an example of the state of the art).

2.2. Modeling of frequency-dependent tissue properties

We next assume that a current pulse $x(t)$ is applied (for example, a square or biphasic pulse). The resulting waveform in the tissue can be found by convolving the pulse with the tissue's impulse response h. If $\boldsymbol{r}$ is the observation point in space, then

$$\varphi(t,\boldsymbol{r}) = x(t) * h(t,\boldsymbol{r}). \tag{2}$$

This can be solved using a frequency-domain solution. The current pulse is first transformed into the frequency domain, giving a spectrum $X(f)$. $H(f,\boldsymbol{r})$ is the calculated electrical potential at each frequency and spatial point generated by a unit amplitude current source. The time domain solution is

$$\varphi(t,\boldsymbol{r}) = \Im^{-1}[H(f,\boldsymbol{r})\cdot X(f)], \tag{3}$$

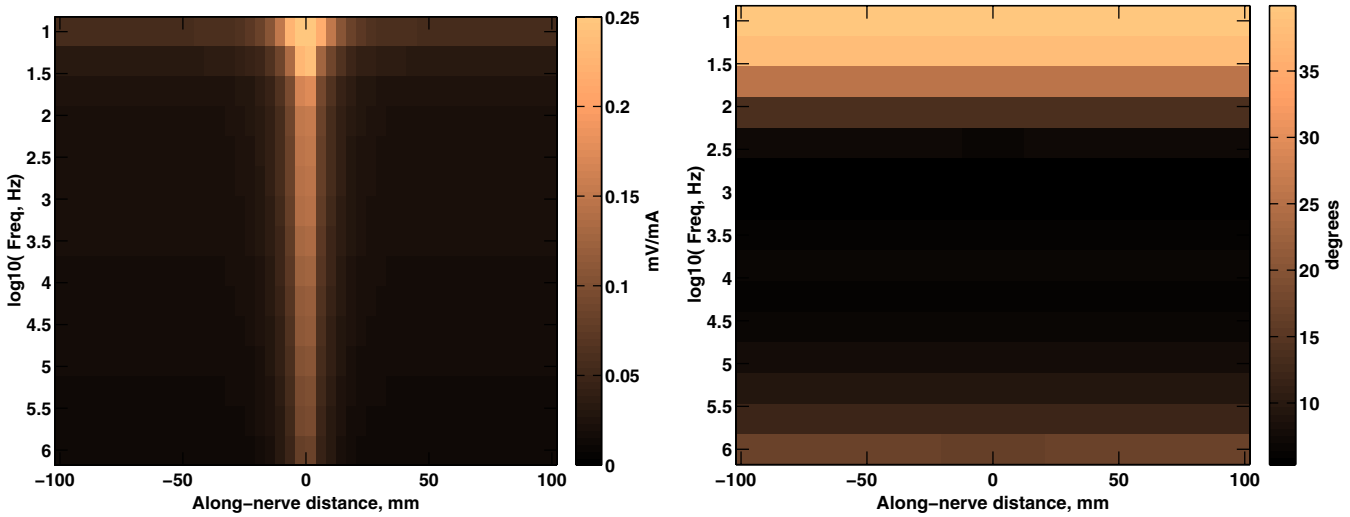

Figure 1. Magnitude and phase of the FEM solution along the axon as a function of frequency (logarithmically spacing) and along-axon distance for a current source at a distance of 5 mm from the midpoint of the axon. Note the smooth variations in magnitude and phase.

where $\Im^{-1}$ denotes the inverse Fourier transform (commonly evaluated using an inverse FFT). Note that $H(f, \boldsymbol{r})$ must be found for every frequency, and that accurately representing the current pulse may require several thousand DFT bins.

Here, an interpolation approach is used to solve (3). The basic observation behind the proposed interpolation approach is that $H(f, \boldsymbol{r})$ is often a slowly varying function of frequency. It is therefore possible to find the solution at a coarse frequency spacing and then interpolate it to the DFT frequency bins. The interpolated unit-amplitude solution can be used in (3) to find the time-domain solution. If there are M bins in the coarse frequency spacing and N DFT bins, the computational savings will be on the order of N/M.

The proposed approach relies on two assumptions. First, the frequency sampling must be sufficiently fine to capture frequency-dependent variations in the magnitude of H. Second, the phase difference between nearby frequencies must be small enough that the phase can be unambiguously interpolated across frequency (this is satisfied if phase differences between neighboring frequencies are $< \pi$; if needed, phase unwrapping can be applied [11]). In detail, the proposed iterative approach is as follows.

(1) Calculate the solution H at a vector $\boldsymbol{f}'$ of coarsely spaced frequencies.
(2) Check for possible phase ambiguities in the result, and unwrap the phase if needed.
(3) Interpolate H calculated at $\boldsymbol{f}'$ to the vector $\boldsymbol{f}$ containing all DFT frequency bins, and use equation (3) to calculate the time-domain waveform.
(4) Calculate the potential at a more finely spaced set of frequencies $\boldsymbol{f}''$ (for example, twice as finely spaced as $\boldsymbol{f}'$).
(5) Repeat steps 2–3 for the frequencies $\boldsymbol{f}''$.
(6) Check for convergence, as determined by the mean-square error between the two calculated time series or a similar metric.
(7) Continue steps above until convergence is achieved.

3. Results

3.1. Model geometry

The interpolation approach was tested using the COMSOL finite element code (COMSOL, Burlington, MA, USA), which was used to model a homogeneous 20 cm long cylinder of 5 cm width. This geometry is similar to that from [5]. Stimulating electrodes, modeled as a point source, were located inside the tissue midway along the cylinder length and at varying depths. To model monopolar stimulation, a 2 cm long region of the tissue exterior, centered midway along the cylinder, was held at ground to provide the return path for the current. Otherwise the tissue exterior was assumed to be electrically insulated. Tissue electrical properties are isotropic, homogeneous and frequency dependent, and were chosen to match gray matter properties from [6]. The neurons were assumed to be located at the center of the cylinder and to be oriented along the long axis of the cylinder.

Point sources were activated one at a time (in different model runs) to investigate the effect of source position. The source was assumed to apply pulses (100 μs typical pulse width) with 1 mA current (note that FEM outputs can be scaled to model other input currents). The input waveform was sampled at 1 MHz. This high sampling rate was used to give an accurate reconstruction of the waveform. For this sampling frequency, there are $N = 2048$ positive DFT bins.

3.2. Numerical results for frequency interpolation

Figure 1 shows the calculated electrical potential $H(f, \boldsymbol{r})$ when the source is 5 mm away from the axon. The potential is calculated at 50 points along the axon, and for 30 frequencies spaced logarithmically between 0 and 0.5 MHz (Nyquist rate). The solution varies smoothly with frequency and has an unambiguous phase, indicating that interpolation should be straightforward. Phase variations in the along-axon dimension are very small.

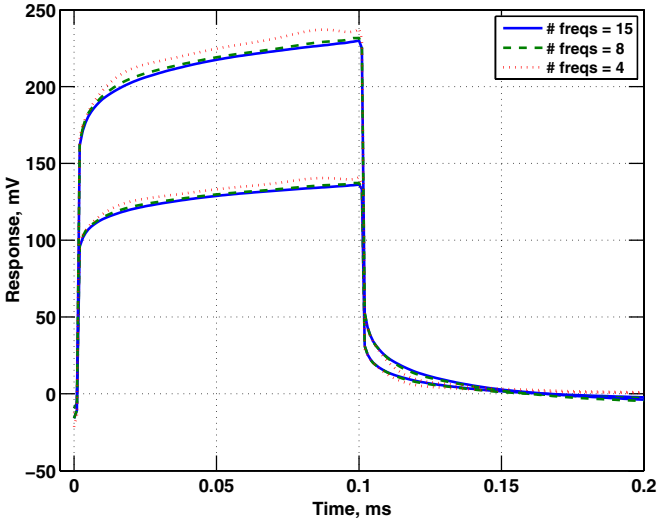

Figure 2. Predicted response to a 0.1 ms pulse at 3 mm (higher curves) and 5 mm from the axon. The interpolation approach is used with 15, 7, and 4 frequencies logarithmically spaced from 1 Hz to 1 MHz.

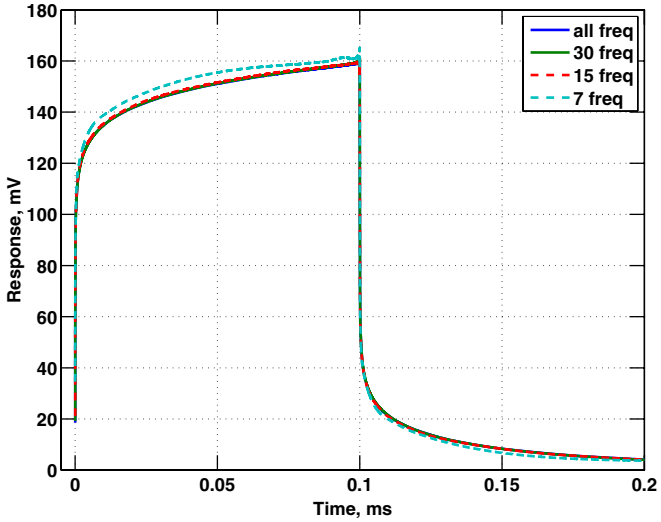

Figure 3. Predicted free-space response to a 0.1 ms pulse at 5 mm distance. Interpolation of 30, 15, and 7 logarithmically spaced frequencies is compared to a solution that is calculated at every DFT bin.

Figure 2 shows the predicted time series created using the iterative procedure outlined above for the needle positions 3 mm and 5 mm from the axon. An initial frequency sampling consisting of 15 logarithmically spaced points in frequency from 1 Hz to 1 MHz was used to generate a first set of results; note the charging/discharging behavior seen at the start and end of the pulse due to tissue capacitance. A downsampled solution with seven frequency points gives very similar solutions. Reducing the number of points to 4 leads to a noticeable increase in the solution error.

While the results in figure 2 indicate that the numerical solution is converging, it would be desirable to use an arbitrarily fine frequency sampling to further check the solution. While this would be computationally demanding for an FEM calculation, the analytic result for a point source in free space [3] can be used to validate the interpolation approach.

Figure 3 shows the calculated results in free space at a distance of 5 mm from a point source. The results of calculating the potential at every DFT bin are compared to solutions found by calculating it at 30, 15, and 7 logarithmically spaced points between 1 Hz and 1 MHz, followed by interpolation. An additional point at 0 Hz is added to capture DC shifts in the solutions. Nearly identical results are seen for 15 and 30 points. As in figure 4, some small differences are seen when the frequency sampling is decreased to seven points. Based on these results, 15 frequency points are used for simulations presented below.

3.3. Numerical results for approximate solutions

Next, the model was set up to find three separate solutions, for the Helmholtz equation (1*a*) and the two quasistatic approximations (1*b*) and (1*c*). For the quasistatic models, the tissue conductivity was specified to be real in the QS-R model (1*c*) or complex in the QS-RC model (1*b*). Typical solutions are shown in figure 4. To demonstrate the flexibility of the calculation approach, results are shown for both monophasic (left) and biphasic (right) stimulation. The change in waveform shape did not require recalculating FEM results; instead, the source spectrum used in equation (3) was recalculated for each waveform.

Helmholtz and QS-RC solutions are indistinguishable, while the QS-R solution does not demonstrate the charging/discharging behavior introduced by tissue capacitance. The rising and falling edges of the QS-R solution are rounded as the frequency-dependent conductivity is explicitly modeled. Tissue conductivity drops with frequency, so the tissue acts as a low-pass filter.

Figure 4 also shows a predicted QS-RC response assuming frequency-dependent conductivity, but frequency-*independent* permittivity (labeled 'QS-RC, constant C'). The frequency-independent permittivity value was found by averaging over frequency, weighted by the magnitude of the source spectrum. Note that the peak amplitude of this solution is essentially identical to the QS-R solution, while the full frequency-dependent QS-RC solution has a higher peak amplitude. This phenomenon and its effects on neural response are discussed below.

The error in the approximate solutions, compared to QS-H, can be expressed as the percentage difference between the various models, averaged over time samples when stimulus is being applied [3]. Using QS-RC as an example, the error is

$$E = 100\frac{1}{N}\sum_{i=1}^{N}\left|\frac{\phi_{\mathrm{QS-RC}}(t_i, \boldsymbol{r}) - \phi_{\mathrm{Helm}}(t_i, \boldsymbol{r})}{\phi_{\mathrm{Helm}}(t_i, \boldsymbol{r})}\right|. \qquad (4)$$

Equation (4) was evaluated for the various solutions as a function of distance to source for monophasic 100 μs pulses. Differences between the Helmholtz and QS-RC model are negligible at all distances (ranging from 0.0003 to 0.0025%) while differences between Helmholtz and QS-R models are roughly 11.8% and are nearly constant with distance (ranging from 11.79 to 11.80%).

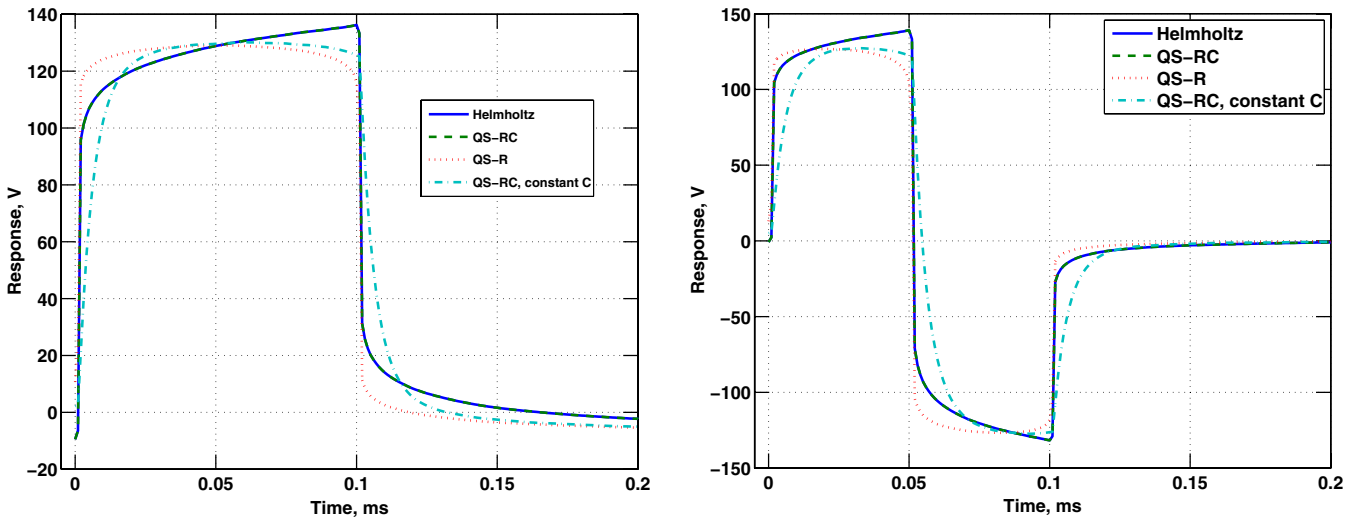

Figure 4. Predicted response to a 0.1 ms pulse at a 5 mm distance under the three approximations to equation (1*a*) considered here. Results are shown for a monophasic stimulation (left) and biphasic stimulation (right). Note that including frequency-dependent conductivity (in QS-R) leads to a rounding of the waveform. The effects of capacitance vary depending on whether capacitance is frequency dependent or frequency independent.

3.4. Computational load

Computation times were measured for the various solutions on a 3.4 GHz PC with 3.5 MB of RAM. A solution of the Helmholtz equation required roughly 18 min for 15 frequencies versus 37 min for 30 frequencies. Extrapolating these values, we estimate that a full direct calculation of 2048 frequencies would have required 41 h.

The differences in computational load for evaluating the Helmholtz solution (equation (1*a*)) versus approximate solutions were also measured. Moving from a real-valued to a complex-valued problem (i.e. from QS-R to QS-RC) caused the runtime to nearly double. However, the runtime for the full Helmholtz solution (1*a*) showed only an insignificant (3%) increase over the QS-RC time. Thus, for problems in which capacitance is important, there appears to be minimal computational penalty for calculating the exact solution.

3.5. Neural activation thresholds

The axon fiber response was described using the well-known Frankenhaeuser–Huxley, or *F–H* model [12]. The transmembrane voltage at the nodes of Ranvier is expressed as a matrix equation [1]

$$c_m \frac{\partial \boldsymbol{V}_m}{\partial t} + i_{\text{ion}} = \boldsymbol{G}\left(\boldsymbol{V}_m + \boldsymbol{V}_e\right), \tag{5}$$

where $\boldsymbol{V}_m$ are the transmembrane voltages and $\boldsymbol{V}_e$ are the external potential values at each node. The first term on the left represents capacitive currents across the membrane, while the second represents the summed ionic currents through ion channels. These ionic currents have a complicated nonlinear behavior that is described by the *F–H* model as found in [12]. The right side represents current flow from adjacent nodes, with $\boldsymbol{G}$ being a tridiagonal matrix expressing the conductance between adjacent nodes.

Figure 5 shows neural activation thresholds for a 20 μm fiber excited by a monophasic 100 μs pulse, modeled using the *F–H* model. The fiber excitation threshold is shown as a function of source-to-axon distance. Thresholds for Helmholtz and QS-RC models (with frequency-dependent capacitance) are indistinguishable. However, interesting differences can be noted by comparing two capacitive solutions to the QS-R solution. Including a frequency-*independent* capacitance has little effect at short distances, but *increases* thresholds by roughly 7% at distances >5 mm. This trend is consistent with results in [5], which noted a decrease in activated brain volume when frequency-independent capacitance was included. In contrast, adding a frequency-*dependent* capacitance *decreases* thresholds by roughly 6% across all distances modeled.

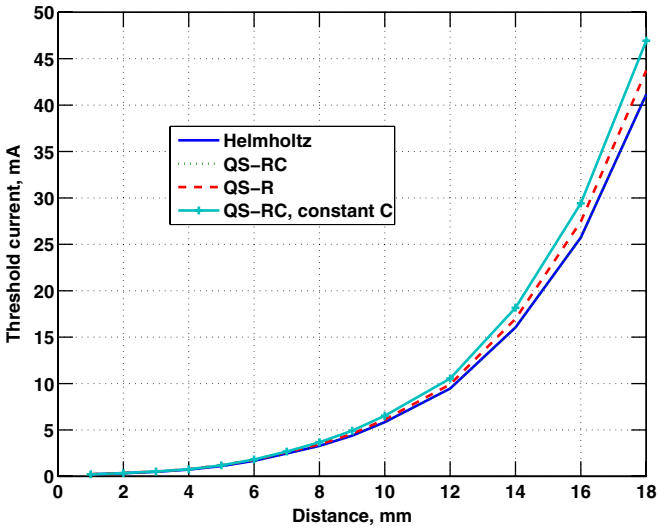

Figure 5. Activation thresholds versus distance from the source for a 20 μm fiber excited using a 1 mA, monophasic 100 μs pulse. Including a frequency-independent capacitive component increases firing thresholds relative to the QS-R solution, while frequency-independent capacitance decreases threshold currents.

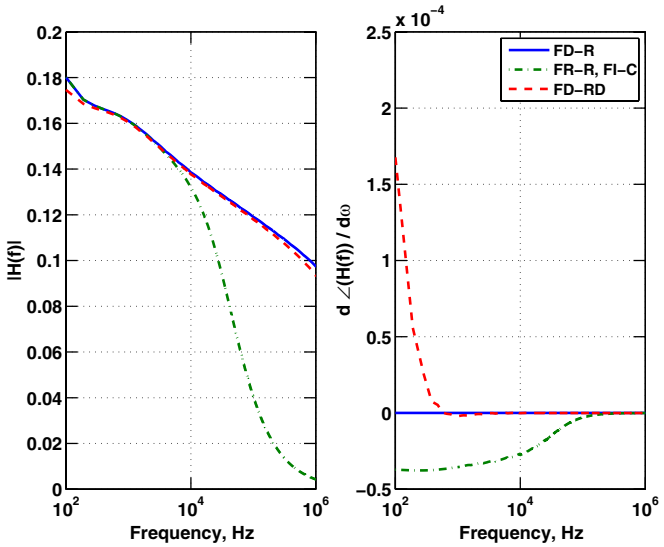

Figure 6. The magnitude and group delay associated with the tissue transfer function (viewed as a filter) are shown for frequency-dependent resistive only solutions (blue), frequency-dependent σ but frequency-independent ε (green) and both σ and ε frequency dependent. Frequency-independent capacitance has the effect of attenuating higher frequency components, while frequency-dependent capacitance distorts the waveform through variable group delay.

This behavior can be explained by viewing the tissue as a filter. In free space, the analytic solution for the field (neglecting propagation effects) is [3]

$$H(f, R) = \frac{I_s}{4\pi R\,[\sigma(f) + \mathrm{i}\omega\varepsilon(f)]},$$

where R is the distance to the source. If the permittivity is frequency independent, its only effect is to attenuate the field. The response magnitude is reduced at higher frequencies (denominator grows), and no signal distortion is introduced, since the linear phase shift $\mathrm{i}\omega\varepsilon$ ensures that the group delay is constant with frequency [13]. This ensures that the addition of a frequency-independent permittivity can only increase thresholds. In contrast, a frequency-dependent permittivity will lead to a nonlinear change in phase with frequency. Thus, variable group delay and signal distortion can be expected. The importance of these effects will depend on the tissue properties.

Figure 6 shows the calculated magnitude and group delay for a freespace source at $R = 5$ mm for the tissue properties used in the FEM model. The frequencies below 10 kHz are of most interest as they contain most of the signal energy for 100 μs pulses. As expected, the frequency-independent permittivity acts to reduce the field magnitude at high frequencies. In contrast, the gray matter permittivity from [6] decays rapidly with frequency and has little effect on field magnitude at higher frequencies, though some attenuation is seen at low frequencies. Differences in the calculated group delay (change of solution phase with frequency) are noticeable. Frequency-independent permittivity causes basically constant group delay over the frequencies of most interest, though the delay does transition to zero as the field magnitude goes to zero. Strong frequency-dependent effects are seen for frequency-dependent permittivity, indicating that signal distortion is expected.

These results help us to explain the waveforms from figure 4. For frequency-independent conductivity, waveform transitions are slower due to attenuation of high frequencies, but peak amplitudes are unchanged. Thus, the total power in the pulse is reduced, which in turn leads to the higher thresholds seen in figure 5. In contrast, dispersive effects cause the solutions with frequency-dependent capacitance to be distorted, resulting in a higher peak amplitude and the lower thresholds seen in figure 5.

4. Discussion

The first set of results above demonstrated that the proposed frequency interpolation approach converges with a relatively coarse frequency sampling. This reflects the relatively slow change in tissue properties with frequency and also the fact that propagation effects (which could introduce phase ambiguities) are negligible over the distances considered. The coarse frequency sampling gives rise to a reduction in computation time of roughly two orders of magnitude compared to a brute-force approach. While of course slower than a frequency-independent solution, the runtime of the interpolation approach is very manageable.

While the interpolation approach above used a simple refinement of frequency sampling (halving the frequency spacing) it would also be possible to adaptively refine the frequency sampling. This could allow regions of rapid variation to be sampled in greater detail, while more slowly varying regions could be sampled more coarsely.

In comparing the different models used, the Helmholtz and QS-RC models gave nearly identical predicted waveform shapes and had very similar computational loads. Much larger differences were seen when comparing a purely resistive (but frequency dependent) QS-R solution to the Helmholtz solution. This reflects the fact that capacitive effects are known to be the most significant effect that is commonly neglected in quasi-static studies. The predicted errors in waveform shape for a 100 μs stimulus were roughly 12% over the distances considered. These values are of the same order of magnitude as those reported in [3] for a problem involving muscle tissue.

The QS-R results above used frequency-dependent values for conductivity, which gave rise to the low-pass filtered appearance of the waveforms (i.e. pulse edges are rounded). More typically, a frequency-independent conductivity value is used. Since tabulated tissue values are frequency dependent, it is not immediately obvious how to pick the best frequency-independent value for modeling. Comparison with a frequency-dependent model, as done in [3], can be helpful in determining an appropriate frequency-independent conductivity value. If this approach is chosen, this interpolation approach described here may be of use in providing a reference solution.

The second set of results above explored differences between frequency-independent and frequency-dependent capacitance. In the former case, capacitance always causes an attenuation of high-frequency field components and does not introduce signal dispersion. In the latter case, signal dispersion can be dominant, as in the examples shown. These

results lead to opposite effects on neuron activation thresholds; while attenuation due to frequency-independent capacitance can only increase thresholds, the dispersion due to frequency-dependent capacitance can cause fibers to fire at lower currents.

This study has several limitations in terms of exploring the effect of capacitance on pulse shape and axon firing thresholds. Electrode-tissue impedance is not included here, but in some cases (especially for surface electrodes) this interface may include a significant capacitive component. Second, the effect of pulse duration was not explored. Earlier work [3] suggests that capacitive effects can become more important for both shorter (<25 μs) and longer (>200 μs) pulses.

It is important to note that, for the cases studied here, the differences in solutions obtained by different models are small compared to uncertainties in actual tissue properties. Also, accurate measurements of frequency-dependent tissue properties are difficult to obtain. The importance of capacitance also depends on the problem at hand; the approach described here was originally developed to model a peripheral nerve stimulation scenario [14], and capacitive effects were less important for the muscle tissues involved in that problem. Thus, for many problems the standard approach of using a frequency-independent model that ignores capacitance may be quite reasonable. However, the conclusions of this paper are that tissue capacitance can be modeled in a computationally efficient manner, and that frequency-dependent properties may have a noticeable effect on model predictions.

5. Conclusion

This paper introduced a frequency-domain interpolation approach that allows frequency-dependent tissue properties to be modeled at reasonable computational cost. Using this framework, the (exact) Helmholtz solution was compared to several quasistatic approximations, in terms of both predicted fields in the tissue and predicted threshold currents for neural stimulation. Results show that previous reports that capacitance leads to higher threshold currents [5] will hold true whenever frequency-independent capacitance is assumed. When frequency-dependent capacitance is assumed, dispersion effects can dominate and may lead to lower threshold currents. These results highlight the importance of accurate measurements of tissue properties.

Acknowledgments

The authors are very grateful to suggestions by the reviewers and editor, which greatly improved the manuscript. They would also like to acknowledge financial support from NeuroMetrix, Inc., where both were employed when the work was performed. Plamen Krastev and Zhixiu Han (both of NeuroMetrix) contributed to modeling discussions, while Walter Frei of COMSOL gave valuable suggestions on field modeling approaches.

References

[1] Kuiken T A, Stoykov N S, Popovic M, Lowery M and Taflove A 2001 Finite element modeling of electromagnetic signal propagation in a phantom arm *IEEE Trans. Neural Syst. Rehabil. Eng.* **9** 346–54

[2] Plonsey R 1969 *Bioelectric Phenomena* (New York: McGraw-Hill) chapter 5

[3] Bossetti C A, Birdno M J and Grill W M 2008 Analysis of the quasi-static approximation for calculating potentials generated by neural stimulation *J. Neural Eng.* **5** 44–53

[4] Troy J and Cantrell D R 2008 A time domain finite element model of extracellular neural stimulation predicts that non-rectangular stimulus waveforms may offer safety benefits *Conf. Proc. IEEE Eng. Med. Biol. Soc. (August 2008)* pp 2768–71

[5] Butson C R and McIntyre C C 2005 Tissue and electrode capacitance reduce neural activation volumes during deep brain stimulation *Clin. Neurophysiol.* **116** 2490–500

[6] Gabriel C, Gabriel S and Corthout E 1996 The dielectric properties of biological tissues: I. Literature survey *Phys. Med. Biol.* **41** 2231–49

[7] Stoykov N S, Lowery M M, Taflove A and Kuiken T A 2002 Frequency- and time-domain FEM models of EMG: capacitive effects and aspects of dispersion *IEEE Trans. Biomed. Eng.* **49** 763–72

[8] Stoykov N S, Kuiken T A, Lowery M M and Taflove A 2003 Finite-element time-domain algorithms for modeling linear Debye and Lorentz dielectric dispersions at low frequencies *IEEE Trans. Biomed. Eng.* **50** 1100–7

[9] Lowery M M, Stoykov N S, Taflove A and Kuiken T A 2002 A multiple-layer finite element model of the surface EMG signal *IEEE Trans. Biomed. Eng.* **49** 446–54

[10] Logothetis N K, Kayser C and Oeterlmann Z 2007 *In vivo* measurement of cortical impedance spectrum in monkeys: implications for signal propagation *Neuron* **55** 809–23

[11] Smith S W 1997 *The Scientist and Engineer's Guide to Digital Signal Processing* (San Diego, CA: California Technical Publishing)

[12] Frankenhaeuser B and Huxley A F 1964 The action potential in the myelinated axon fibre of *Xenoupus Laevis* as computed on the basis of voltage clamp data *J. Physiol.* **171** 302–15

[13] Oppenheim A V and Schafer R W 2009 *Discrete-Time Signal Processing* (Englewood Cliffs, NJ: Prentice-Hall)

[14] Tracey B H, Krastev P, Han Z and Williams M 2009 Computational modeling of peripheral nerve stimulation *Conf. Proc. IEEE Eng. Med. Biol. Soc. (September 2009)* pp 6777–80